Cement and Concrete Research 100 (2017) 129–139

Contents lists available at ScienceDirect

Cement and Concrete Research

journal homepage: www.elsevier.com/locate/cemconres

Investigation on a green olivine nano-silica source based activator in alkali activated slag-fly ash blends: Reaction kinetics, gel structure and carbon footprint

X. Gao[a,b], Q.L. Yu[b,*], A. Lazaro[b], H.J.H. Brouwers[a,b]

[a] State Key Lab of Silicate Materials for Architectures, Wuhan University of Technology, Wuhan 430070, PR China
[b] Department of the Built Environment, Eindhoven University of Technology, P.O. Box 513, 5600 MB Eindhoven, The Netherlands

ARTICLE INFO

Keywords:
Olivine nano-silica
Alternative activator
Alkali activation
Slag-fly ash blends
CO_2 footprint
NMR

ABSTRACT

In this paper, a green olivine nano-silica is synthesized and applied as an alternative silicate source to prepare alkali activators, and a commercial waterglass based silica source is studied as a reference. The synthesis route and characterization of olivine nano-silica is presented. The effects of silicate origin and dosage on activator characteristics, reaction kinetics, gel structure and strength are investigated and the CO_2 footprint is evaluated. The results show that increasing the activator modulus significantly increases the high crosslink Q contents in the alkali solution, nano-silica based ones exhibit slightly higher percentages of Q3 sites. Nano-silica based mixes exhibit comparable properties regarding the reaction intensity, chemically bound water content and strength. Gel compositions of both nano-silica and waterglass based samples are characterized in detail by using solid ^{29}Si and ^{27}Al MAS NMR. Moreover, replacing commercial waterglass by this alternative silicate source reduces the CO_2 emission between 20.4% and 29.0%.

1. Introduction

The production of ordinary Portland cement (OPC) is accompanied with a number of environmental issues such as carbon emissions, consumption of natural clays and high energy costs. In order to reduce those negative impacts, great attention has been paid to applying alkali activated materials as alternatives to Portland cement. This type of material generally exhibits reduced energy costs and carbon emissions [1,2] together with excellent mechanical properties, durability and thermal resistance [3–6]. Two typical binding systems can be classified based on the chemical composition and the reaction mechanism of the starting materials: One is the Si + Ca system, having C-A-S-H type gel as the main reaction product [7]; another is the Si + Al system, having N-A-S-H type gel within a three-dimensional network as the major reaction product [8]. The typical precursors for these two systems are slag and metakaolin/class F fly ash, respectively [1,8].

Growing efforts have been spent on the blended alkaline system recently. Due to the fact that mixing calcium enriched aluminosilicates dominated precursors results in a series of modified properties including the setting times, workability, shrinkage, mechanical properties and durability [9–12]. Micro-scale analyses reveal that the reaction products are stable coexisting C-A-S-H and N-A-S-H type gels [13–15], indicating a desirable gel compatibility. Besides, the effects of key synthesizing factors such as activator type and dosage, raw materials' composition and curing conditions on reaction kinetics, gel characters, mechanical properties and durability issues have been also intensively investigated [16–20].

In terms of the alkali activators, it is widely accepted that a mixture of silicates and caustic alkalis ($M_2O{\cdot}nSiO_2$ + MOH, where M often refers to Na or K) results in the best mechanical properties and lowest porosity [3,21] compared with other types of activators, and the most commonly used cation is Na due to its relatively low cost and availability. This mixed activator benefits the reaction process by offering alkaline conditions in a moderate and continuous manner, meanwhile providing extra silicate sources that contribute to the formation of reaction products [22]. However, the sodium silicate based activator is the main contributor of energy consumption and carbon emission in alkali activated materials [23]. The production of sodium silicates includes the melting of sodium carbonate and quartz sand at high temperatures (usually around 1400 to 1500 °C), and this process results in a total carbon dioxide release of 403 to 540 kg/ton and an energy consumption between 420 and 1250 MJ/ton [24]. Moreover, the estimated cost of one ton of equivalent silica from commercial sodium silicate solution is currently > 2100 USD [25].

* Corresponding author.
E-mail address: q.yu@bwk.tue.nl (Q.L. Yu).

http://dx.doi.org/10.1016/j.cemconres.2017.06.007
Received 14 March 2017; Received in revised form 11 May 2017; Accepted 29 June 2017

Therefore, in order to obtain a more sustainable alkali activated binder, it is of great interest to design new alkali activators with reduced environmental impacts and lower costs. Exploring alternative silicate in the activator has been proven to be an effective approach. Rodriguez et al. [26] used chemically modified nano-silica and MOH to activate class F fly ash; Zivica et al. [27] applied modified silica fume as alternative activator in alkali activated slag; Puertas et al. [21] developed a mixed activator by dissolving industrial glass waste in NaOH/Na_2CO_3 solution and used it in alkali activated slag; Bernal et al. [28] prepared silicate based activators by mixing silica fume or rice husk ash with NaOH to activate metakaolin/slag blends. These researches show that alternative silicate based activators could provide comparable mechanical properties and similar micro scale characters compared with commercial sodium silicate based resources. However, there are limited mechanism studies regarding the effect of alternative silicates as activator on the blended alkaline system.

On the other hand, the olivine nano-silica, produced by the dissolution of olivine, exhibits advantages with regard to carbon emission, energy consumption and total costs [29]. This type of amorphous nano-silica is produced under temperatures lower than 95 °C and can have a specific surface area between 100 and 400 m^2/g and primary particles as low as 10 nm [30]. Thus it indicates the potential as a sustainable silicate source in the preparation of alkali activators while providing desirable reactive silica. The objective of this study is to evaluate the olivine nano-silica as an alternative activator in alkali activated slag-fly ash blends. The effects of olivine nano-silica on activator characteristics, reaction kinetics, mechanical property and the structure of reaction products are analyzed. Micro-scale analyses are carried out by using an isothermal calorimeter, ^{29}Si and ^{27}Al MAS NMR spectroscopy and thermo-gravimetric/differential scanning calorimeter; and furthermore the total carbon emission of the related mixtures is computed.

2. Experiment

2.1. Materials

The solid precursors used in this study were ground granulated blast furnace slag (GGBS, provided by ENCI, the Netherlands) and a commercial Class F fly ash. Their major chemical compositions were analyzed by X-ray fluorescence, as shown in Table 1. The X-ray diffraction patterns of the used slag and fly ash are shown in Fig. 1, which were measured by using a Cu X-ray tube with a step size of 0.02° and a 2θ range from 15° to 55°. The slag shows a peak hump between 25 and 35° due to the amorphous components and no significant crystalline phases were observed; while the fly ash has an amorphous hump between 15 and 30° and contains crystalline phases such as quartz (SiO_2), mullite ($Al_6Si_2O_{13}$), magnetite (Fe_3O_4) and hematite (Fe_2O_3). Concerning the alkaline activators, analytical level of sodium hydroxide pellets (99 wt %), a commercial sodium silicate solution (27.69% SiO_2, 8.39% Na_2O and 63.92% H_2O by mass) and laboratory prepared olivine nano-silica (19.04% SiO_2 and 80.96% H_2O by mass) were used; the olivine nano-silica was produced by dissolving olivine in acid at low temperatures,

Table 1
Major chemical composition of GGBS and fly ash.

Oxides (wt%)	FA	GGBS
SiO_2	54.62	30.23
Al_2O_3	24.42	12.58
CaO	4.44	40.51
MgO	1.43	9.05
Fe_2O_3	7.21	0.60
Na_2O	0.73	–
K_2O	1.75	0.43
SO_3	0.46	3.47
LOI	2.80	1.94

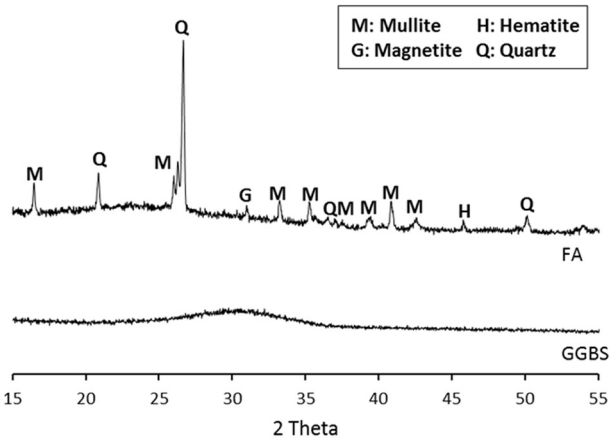

Fig. 1. XRD patterns of GGBS and fly ash.

followed by a washing and filtering process, and the detailed synthesizing route and characterization is presented in Section 3.1. Reference activators with desired modulus were prepared by adding the appropriate amount of sodium hydroxide pellets into the sodium silicate solution. Distilled water was used in order to reach the desired water/binder ratios. Alkali activators with the same activator modulus were prepared by mixing sodium hydroxide pellets with olivine nano-silica and water to achieve the same chemical compositions as the references. The mixed activator solution was cooled down to room temperature prior to further use.

2.2. Experimental program

The activators used in this study had an equivalent sodium oxide (Na_2O) content of 5% by mass of the solid precursors, and the water/binder ratio was kept constant as 0.4 in all mixtures. The water consisted of the added distilled water and the water contained in the activator solution. The chosen Na_2O content and water/binder ratio were taken from the previous studies that ensure sufficient alkalinity without efflorescence and satisfying flowability, respectively [31,32]. The slag/fly ash mass ratio was fixed at 70/30 and three levels of activator modulus (1.8, 1.4 and 1.0) were used. The detailed information of the mix proportions is listed in Table 2 (where WG and NS represent commercial waterglass and olivine nano-silica, respectively).

The reaction kinetics was studied by using an isothermal calorimeter (TAM Air, Thermometric) for the first 72 h under a constant temperature of 20 °C. The solid raw materials were firstly mixed with the activating solution externally and vibrated for about 1 min, then the paste was injected into the ampoule and loaded into the calorimeter.

The compressive strength tests were carried out according to EN 196-1 [33], and each obtained value is an average of three specimens. Samples were prepared using a laboratory mixer; firstly the solid raw materials were added, followed by the activating solution. The fresh samples were casted into plastic molds covered with a plastic film for the first 24 h, then demolded and cured at a temperature of 20 °C and a relative humidity of 95% until their testing age.

Table 2
Mix proportions of alkali activated slag-fly ash composites.

Activator			Solid raw materials		w/b
Type	Na_2O	Ms	Slag	Fly ash	
A: WG + NaOH	5%	1.8	70	30	0.4
B: NS + NaOH		1.4			
		1.0			

The thermo-gravimetric and differential scanning calorimeter (TG/DSC) analysis was conducted using a STA 449 F1 instrument, finely ground powder samples after 3 months of curing were heated up to 1000 °C at a rate of 10 °C/min with nitrogen gas as the medium. Solid-state MAS NMR spectra were carried out using a Bruker Avance 400WB spectrometer, after 3 months of curing. The ^{29}Si NMR spectra were collected at 79.5 MHz on a 7 mm probe, with a pulse width of 6.5 μs, a spinning speed of 15.9 kHz and a relaxation delay of 10 s. The ^{27}Al MAS NMR spectra were obtained at 104.5 MHz on a 4 mm probe, with a pulse width of 6.5 μs, a spinning speed of 41.7 kHz and a relaxation of 2 s.

3. Results and discussion

3.1. Synthesis and characterization of olivine nano-silica

An alternative synthesis route to achieve amorphous nano-silica is the dissolution of silicate minerals in acid. The dissolution of olivine is a competitive alternative route compared to the existing methods of nano-silica production, due to the cheaper and greener process of olivine dissolution at low temperatures. The raw materials employed in this method are olivine ($(Mg,Fe)_2SiO_4$) and sulfuric acid. Olivine (an olivine gem-stone can be seen in Fig. 2(a)) is the most common silicate mineral in the upper mantle and a common mineral in the earth's crust, which makes it a low-price commodity (currently between 75 and 150 USD/ton depending on the quality, location of the quarry and market oscillations). Amorphous silica can be produced through the following reaction (between 50 and 95 °C) [34]:

$$(Mg, Fe)_2SiO_4 + 4H^+ = Si(OH)_4 + 2(Mg, Fe)^{2+},\ 223\ kJ/mol \quad (1)$$

The dissolution yields a slurry consisting of a mixture of magnesium/iron salts, amorphous silica, unreacted olivine and inert minerals. Once the reaction is complete, the unreacted olivine and inert minerals are removed from the final suspension by sedimentation. Subsequently, the silica can be cleaned from the resulting mixture by washing and filtering. After the filtration, a cake with around 20 wt% solid content of nano-silica is obtained. The synthesizing process is briefly presented in Fig. 3.

The produced olivine nano-silica has a specific surface area between 100 and 400 m^2/g, primary particles between 10 and 25 nm (agglomerated in clusters) and silica content above 99%. The particle sizes and a typical TEM picture of produced olivine nano-silica are shown in Fig. 2(b), nano particles with angular shape can be observed.

In addition to the low temperature feature of this procedure (below 95 °C), it should be noticed that the process is exothermic with a reaction heat of 223 kJ per mole of olivine [58]. The energy generation during the olivine nano-silica process for the hypothetical case of an adiabatic reactor is shown in Table 3, the used heat capacity of 25% sulfuric acid is 3.38 $J \cdot g^{-1} \cdot °C^{-1}$ according to [59], while the forsterite and dunite have the similar value of 0.83 $J \cdot g^{-1} \cdot °C^{-1}$ [35]. When 1.5 mol of olivine react with 1 L solution of sulfuric acid 25%, the temperature of the mixture will increase 79 °C. Therefore, the reaction generates more than enough energy to keep the system at the desired temperature (between 50 and 95 °C) provided the reactor is sufficiently insulated. In addition, the dissolution of concentrated sulfuric acid also generates a considerable amount of heat.

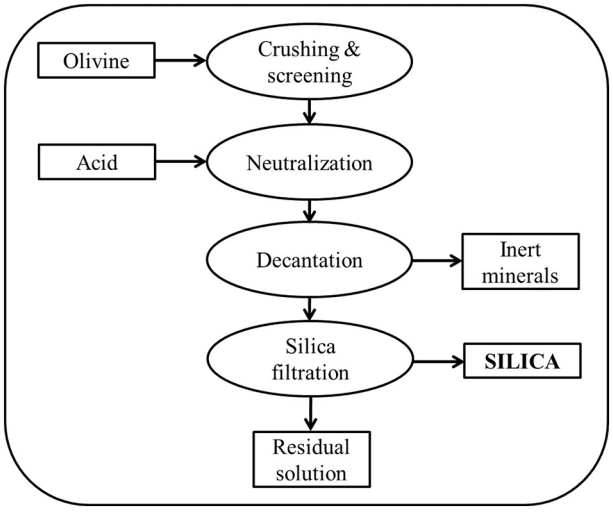

Fig. 3. Chart flow of the olivine nano-sililca production.

Table 3
Energy generation during the olivine nano-silica process.

ΔH_r (kJ/mol)	V_{H2SO4} (L)	m_{H2SO4} (g)	n_{ol} (mol)	m_{du} (g)	X (%)	Q (kJ)	ΔT (°C)
223	1	1186	1.5	242	100	333.5	79.3

ΔH_r is the enthalpy of reaction, X the conversion degree of the reaction and Q is the heat generated. Heat capacities of 25% sulfuric acid and forsterite are 3.38 [67] and 0.83 [35] $J \cdot g^{-1} \cdot °C^{-1}$, respectively. The heat capacity of dunite has been approximated as the one of forsterite.

3.2. Activator characterization

3.2.1. Soluble content

The olivine nano-silica based activators are then produced by mixing the prepared nano-silica cake with sodium hydroxide pellets and distilled water. It is commonly known that the silicates in both cases are mostly soluble silica; and differences in the silicate structure and pH might occur due to the origin of the silica source and the synthesizing parameters. The particle size distributions of the applied

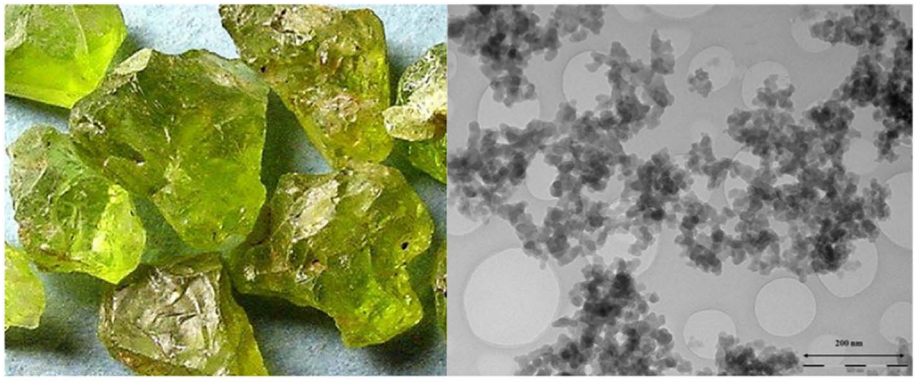

Fig. 2. A sample picture of the olivine gem-stone and a TEM image of produced olivine nano silica [25].

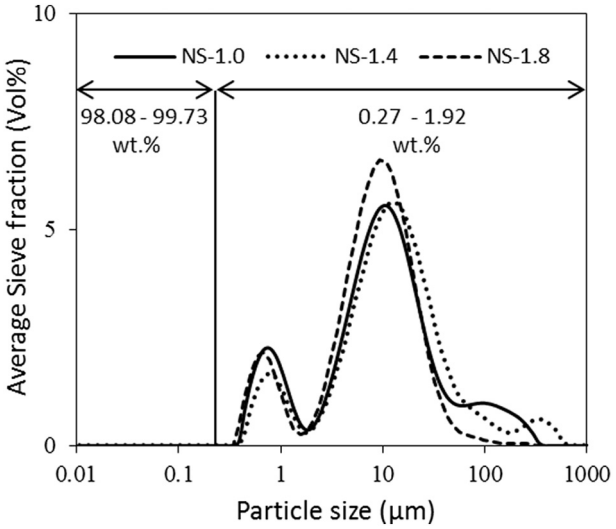

Fig. 4. PSDs of the olivine nano-silica based activators.

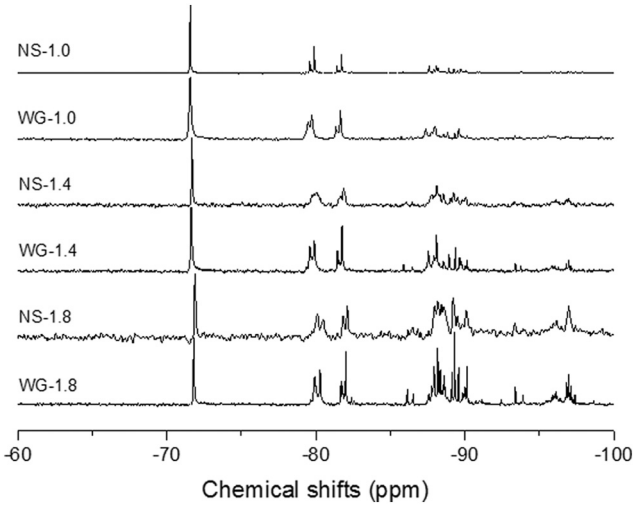

Fig. 5. Liquid ^{29}Si NMR spectrum of activators.

activators are shown in Fig. 4. It can be seen that the un-dissolved silicates show particle sizes are centered at about 10 μm and some small fractions at around 0.8 μm, while no particle sizes are shown below around 200 to 300 μm. Then a 200 nm filter is used in order to identify the mass fractions of the dissolved silicates, since those dissolved ones show no information from the particle size measurement, the results are also shown in Fig. 4. It can be seen that the mass fraction of solids below 200 nm in activators with Ms. of 1.0, 1.4 and 1.8 is 99.88%, 99.73% and 98.08%, respectively. According to [34], when the activator modulus is lower than 2, there are no (or almost none) polymeric silica species (< 2 nm); and the silica species are completely dissolved when the modulus is lower than 1. Thus, it can be concluded that the silica in an olivine nano-silica based activator is almost completely dissolved for Ms. of 1.0 and 1.4, and the sample with a Ms. of 1.8 also reaches a high value of above 98%. It should be noted that there is a slight increase in the soluble solid content when lowering the activator modulus, which suggests again that higher alkalinity (pH) favors the dissolution of silicates. For the undissolved silicates, all the three samples present similar particle size distributions, i.e. a main particle size at around 9.8 μm together with a small amount of particles at about 0.7 μm. These micro particles could be practically the impurities from the olivine. But considering the small mass fraction within the total amount of input silicate (0.27% to 1.92%), their influence should be limited.

3.2.2. pH value

The measured pH values of all the six prepared solutions are shown in Table 4, each value is an average of three measurements. For the nano-silica based activators, very similar pH values are shown in general compared to the waterglass based ones with the same activator modulus, showing that the modulus exhibits a much greater influence than silicate origin in terms of the pH value. While as the modulus increases from 1.0 to 1.8, there is a gradual decrease of pH from 13.48 to 13.19, although those values will represent a high level, the pH variation is significant enough to cause changes in silicate solubility [36,37] and consequently, reactivity of the activator. To summarize, the olivine nano-silica based activators are able to provide comparable amounts of soluble silicate and alkalinity to the commercial waterglass based ones, thus similar macro performances upon activation can be expected.

Table 4
pH values of the activator solutions.

Mix	pH
WG-1.0	13.49
WG-1.4	13.41
WG-1.8	13.17
NS-1.0	13.48
NS-1.4	13.39
NS-1.8	13.19

3.2.3. Liquid ^{29}Si NMR

Liquid ^{29}Si NMR was performed to all the six activators and the results are shown in Fig. 5. For activators with a modulus of 1.0, a significant sharp peak is located at around −72 ppm, indicating the presence of Q0 [38] monomers. Q1 dimers and Q2 trimers at around −80 and −82 ppm are observed [39,40], as well as a certain fraction of Q2 and Q3 groups at about −85 to −90 ppm [41,42]. No significant peaks are shown in ppm ranges lower than −100, suggesting no Q4 sites are present in the activator. When increasing the modulus to 1.4, the intensity of peaks at around −85 to −90 ppm (Q2/Q3 sites) becomes more evident, indicating the increasing fraction of Q2 and Q3 units within the activator solution. Also the Q3 groups that are located at around −95 to −100 ppm start to present. Further increment of the activator modulus to 1.8 results in a more significant peak intensity at around −85 to −90 ppm and −95 to −100 ppm, suggesting an increased amount of Q2/Q3 and Q3 groups within the solution. These chemical shifts can be directly linked to the increment of the activator modulus, which lowers the pH and therefore reduces the silica solubility, resulting in activator solutions with more polymerized silicates. Concerning the effect of silica origin, with a fixed activator modulus, olivine nano-silica derived activators exhibit the same typical peak locations compared to the commercial waterglass based ones, with slight differences in peak intensity and covered area, indicating a similar silicate structure composition in general. In order to further quantify the different silicate groups' fractions, an evaluation on the covered area of identified peak was carried out by using the software MestRec, and the results are listed in Table 5. It should be pointed out that the quantified calculation method is still open for discussion, and can only be used as an indication to show the structural differences. It shows that as the activator modulus increases, there is a general reduction of the low polymerized Q0 and Q1 groups, which usually present higher reactivity than the Qn sites with higher n values. Meanwhile, the Q2 and Q3 contents show a significant increase. With a constant activator modulus, the olivine nano-silica based activators show slightly lower contents of Q0 and Q1 groups, and relatively high fractions of Q2 and Q3 groups. Those slight but detectable structural differences may influence the properties of the resulting alkali activated materials.

Table 5
Evaluation of the silicate structure compositions in alkali solution.

Sample	Q sites and percentage (%)				
	Q0 (−72 ppm)	Q1 (−80 ppm)	Q2 (−82 ppm)	Q2/Q3 (−85 to −90 ppm)	Q3 (−90 to −100 ppm)
NS-1.0	30	21	17	32	0
WG-1.0	32	23	16	29	0
NS-1.4	17	18	13	42	10
WG-1.4	20	21	16	37	6
NS-1.8	7	6	5	54	28
WG-1.8	9	14	10	49	18

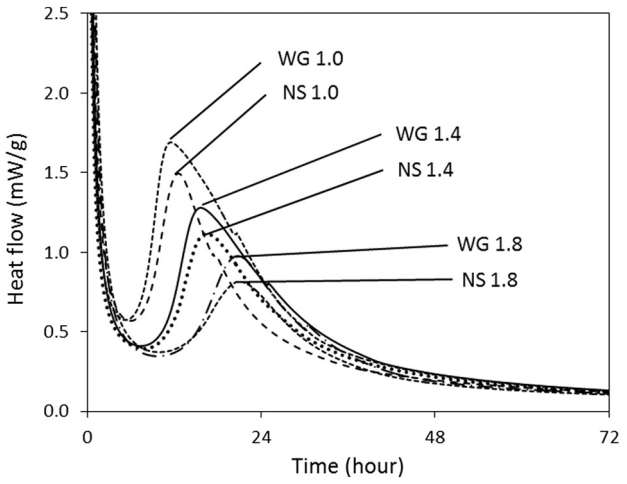

Fig. 6. The normalized heat flow of alkali activated slag-fly ash blends with different activator conditions.

3.3. Reaction kinetics

The isothermal calorimetric analyses were conducted to all six mixtures and the results are illustrated in Fig. 6, following the typical four stages of initial dissolution, induction, acceleration/deceleration and stable period [43–45]. When sodium silicate is used as the activator, two typical calorimetric peaks are usually shown: an initial peak with a significantly high heat flow during the first few minutes (not shown in this study due to the much higher peak intensity) and a heat release peak during the acceleration stage with a relatively low intensity in the following hours. The first peak mainly corresponds to the initial wetting and dissolution of the starting precursors within the first few minutes after mixing [46]; while the second peak is assigned to the massive formation of reaction products [47].

It can be seen from Fig. 6 that for the commercial sodium silicate based samples, the second heat evolution peak appears at around 12 h with an activator modulus of 1.0; as the activator modulus increases to 1.8, this peak shifts to approximately 20 h with a lower intensity. The prolonged induction stage with broader curves also indicates the decreased reaction intensity due to the increase of activator modulus. A similar tendency is also shown in nano-silica based mixes. The more intensive reaction process due to the reduction of activator modulus is also found in the previous investigations [48,49]. The peak change is primarily due to the increased silicate content in the activator solution and the resulted lower pH. When activators with lower moduli are used, the soluble silica exhibits a less polymerized structure in the solution than the ones with higher modulus due to the increased pH [50], thus a more direct interaction between the soluble silicates, alkali solutions and the raw materials is resulted. Besides, due to the silicate equilibrium based on the pH, the increased soluble silicate content at the beginning stage may negatively influence the dissolution of the silicate units from the original slag, consequently leading to an increased reaction time.

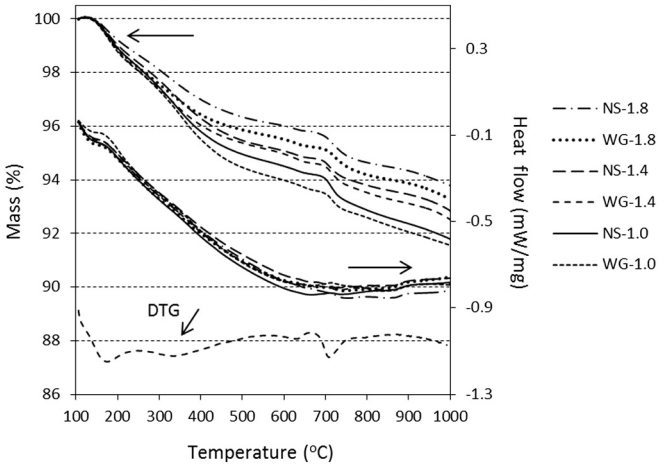

Fig. 7. TG/DSC analyses of all mixes, after 3 months of curing.

Concerning the nano-silica based mixtures, for each fixed activator modulus, the location of the main reaction peak slightly shifts to longer times. Besides, the peak intensities of those mixtures are slightly lower than the commercial sodium silicate based ones, together with less covered areas in all cases. It reveals that nano-silica based samples present a slightly less intensive reaction process during the first 72 h. Considering the facts that in the olivine nano-silica based activators, small fractions of the undissolved materials are present; slightly lower pH for a constant modulus is shown; and relatively high content of polymerized Q groups is exhibited, these could explain the slightly reduced reactivity compared to the commercial sodium silicate activators.

3.4. Gel structure

3.4.1. TG/DSC

The thermal analyses of the mixes with different silicate sources and activator moduli are presented in Fig. 7. Special attention is paid to the reacted gels and the initial mass after holding at 105 °C for 1 h is calculated as the starting mass (i.e. 100%), in order to analyze the structural changes at elevated temperatures. All the samples are cured for 3 months. It can be seen that after a negligible mass loss between around 105 and 160 °C, all mixtures exhibit a gradual mass decrease until 1000 °C. Between the temperature range of around 160 and 800 °C, all samples exhibit similar tendencies of mass loss, a representative DTG curve from sample WG-1.4 is shown in the figure, revealing four peaks that correspond to the gradual decomposition of the C-A-S-H type gels (about 160 °C); hydrotalcite type phases (around 330 °C) and carbonates (around 620 and 710 °C), respectively [15,37,51]. The DSC results show two heat absorption peaks at around 160 and 700 °C (small shoulder), corresponding to the decomposition of reacted gel and carbonates [52], respectively. Besides, there are no other abrupt mass losses between 105 and 1000 °C, which reveal that the reaction products in this case are mainly amorphous gels with chemically bound water, while certain amount of carbonates are formed caused by the carbonation.

For a constant activator modulus, samples prepared using commercial sodium silicate exhibit a larger mass loss than the olivine nano-silica based ones between 105 and 1000 °C; and mixes with a higher activator modulus show a lower total mass loss in general. Specifically, in olivine nano-silica based samples, the mass loss after 105 °C is around 8.2%, 7.2% and 6.2% for mixes with an activator modulus of 1.0, 1.4 and 1.8, respectively. The corresponding values for sodium silicate based mixtures are 8.4%, 7.5% and 6.7%. The slight but noticeable difference in mass loss indicates that slightly more chemically bound water/reaction products are formed in commercial sodium

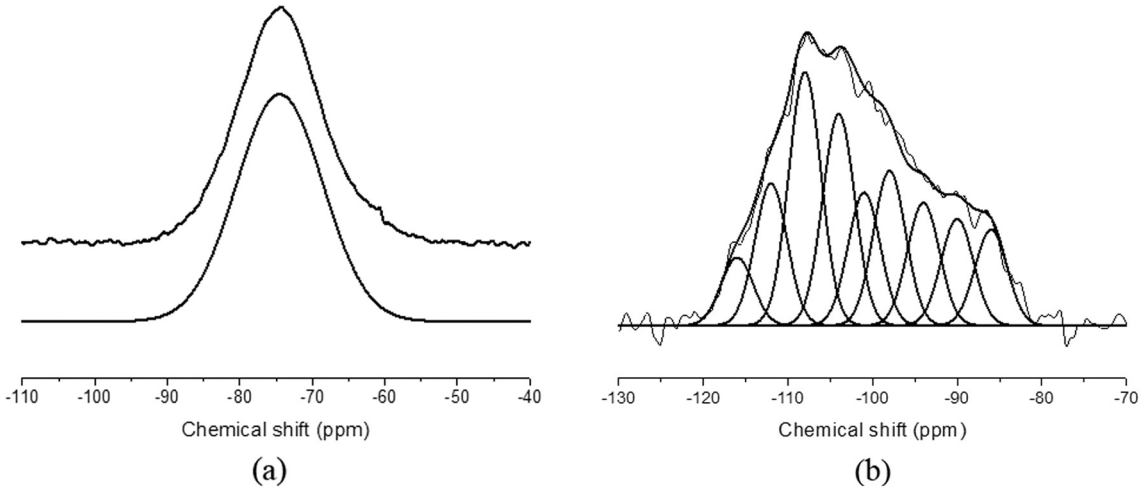

Fig. 8. ^{29}Si MAS NMR of starting materials (a: slag; b: fly ash).

silicate based mixes, and a lower activator modulus benefits the reaction rate. These results are well related to the calorimeter results in this study, where the olivine nano-silica derived mixes exhibit less intensive reaction, and a higher activator modulus (higher amount of additional silicate from activator) slows down the reaction to some extent. Therefore, it is reasonable to state that the olivine nano-silica based activators present a very slightly lower activation efficiency compared to the commercial sodium silicate based ones, which is attributed to the silicate origin. Besides, the mass loss between 650 and 800 °C is about 1.04% to 1.39%, which mainly includes the decomposition of carbonates and a small amount of chemically bound water, which provides a qualitative identification about the carbonation behaviors of this blended alkali system.

3.4.2. ^{29}Si MAS NMR

Fig. 8 shows the ^{29}Si MAS NMR spectra of the unreacted slag and fly ash. The unreacted slag exhibits a broad peak in the range between − 55 and − 95 ppm, centered at around − 75 ppm. The later deconvolution work on the spectra was carried out according to [39,40], the contour of the raw slag after alkali activation is assumed to be unchanged, and its spectrum range is fixed and the intensity is rescaled by a certain factor to evaluate the contribution of raw slag in the corresponding overlapped areas. The location and width of the deconvoluted peaks were kept constant throughout the study, with minimized number of possible peaks. The spectrum of the unreacted fly ash presents a broad overlapped peak within the range of − 80 and − 120 ppm, assigning to the Q4 structures with different aluminate substitutions: Q4(mAl), m = 0–4. The deconvolution of the overlapped peaks in fly ash is carried out in Origin Pro 9.0 by applying the Gaussian line model, constant peak widths and locations are used throughout the whole study. Peak locations and physical meanings are based on the analytical results from the software and the available literatures [37,39,53,54].

Figs. 9 and 10 show the ^{29}Si MAS NMR spectra of slag-fly ash blends activated by commercial sodium silicate solutions and olivine nano-silica based ones after 3 months of curing, respectively. The fitting peak and deconvoluted peaks are presented below the obtained spectra in each figure. After activation, all mixes show obvious spectra of slag and Q4(mAl) sites, indicating the presence of unreacted slag and fly ash. It should be noted that a small scaled formation of N-A-S-H gels (Q4 structures) may also occur and the resulting spectra are overlapped with the original fly ash and Q3(1Al) groups (around − 80 to − 120 ppm), making those phases difficult to quantify [39,40]. However, the main newly formed phases within the range of − 70 to − 90 ppm are relatively easy to distinguish. The deconvoluted peak located at around − 75.2 ppm refers to the Q0 sites, two Q1 peaks (non-bridging structure, Q1-a, and Q1-b) are identified at about − 76.8 and − 79.0 ppm, since a single Q1 group is not sufficient to reach an ideal peak fitting. Previous studies also observed two Q1 sites types in the C-(A)-S-H type gels, while the differences in the chemical environments of these two groups are not specified [40,55]. Peaks at approximately − 81.6, − 84.2 and − 85.7 ppm are attributed to the bridging Q2(1Al), Q2-b, Q2-p sites within the C-(A)-S-H gels, respectively. Three different Q2 sites are also reported in previous studies [67]. Besides, three sites show an overlapped location at around − 85 to − 90 ppm, including two Q4(4Al) groups that are observed in the original fly ash and a newly formed Q3(1Al) groups; the strong presence of relatively high crosslink Q3(1Al) sites in alkali activated slag and its blends is also observed in the available literatures [55,53,56].

The effect of activator modulus and alternative silica on gel structure is quantified based on the deconvolutions and the results are summarized in Table 6. The reaction degree of slag (RD, in terms of Si) is calculated as follows (in mol%):

$$RD = \frac{Si(Or) - Si(Un)}{Si\,(Or)} \times 100\% \quad (2)$$

where Si(Or) is the input Si from the original slag, and Si(Un) is the unreacted Si in slag within the reaction products. When increasing the activator modulus from 1.0 to 1.8, the slag reactivity gradually decreases from about 72% to 58% in both commercial sodium silicate and olivine nano-silica based mixes. This result is in line with the isothermal calorimetric and thermal analyses in this study that a lower activator modulus favors a more intensive reaction process, which leads to an increased bound water content; and with a same activator modulus, olivine nano-silica derived mixes present a slightly lower reaction degree compared to the commercial ones. The Q0 content slightly decreases with the increase of activator modulus in olivine nano-silica based samples, while it remains stable in waterglass based ones. Regardless of the silica origin and activator modulus, the content of Q1 and Q2 groups only shows slight shifts; the stable content of Q4(0-3Al) groups may suggest a limited but constant contribution of fly ash during activation.

The most evident structural change is observed in the Q2(1Al) groups, namely the increase of activator modulus results in a decrease of around 5% within the studied parameter range in this case, while the effect of silica origin is not obvious. It should be noted that the starting precursors (slag and fly ash) are the only aluminate sources in this case, and slag presents a dominant effect in providing aluminate considering its content and reactivity. Thus it is reasonable to conclude that the reduction of Q2(1Al) sites is attributed to the decreased content of reacted slag and therefore less Al is available for the reaction. Another obvious structure shift is the high crosslink Q3(1Al) + Q4(4Al) sites,

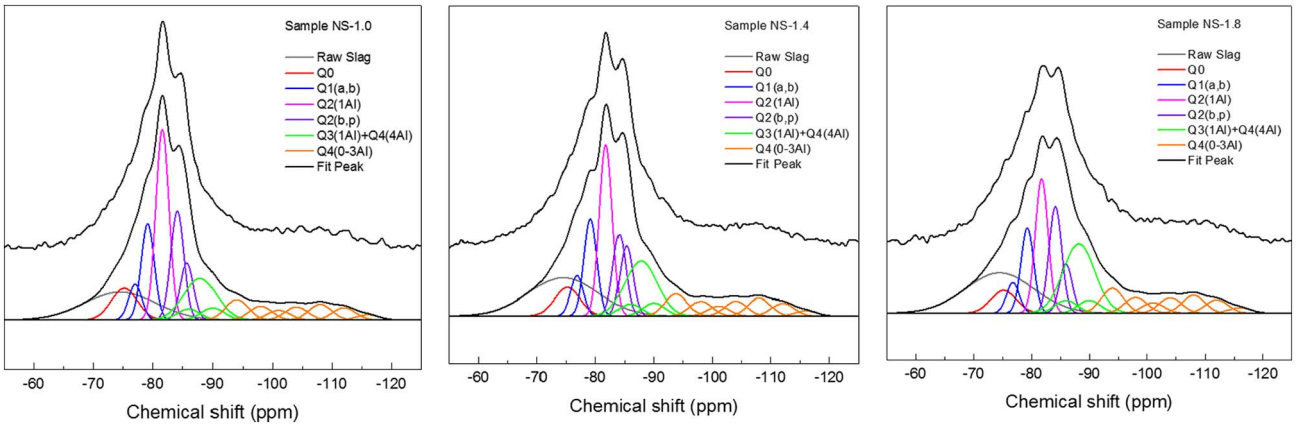

Fig. 9. ^{29}Si MAS NMR of mixes based on olivine nano-silica.

their content is stable in commercial sodium silicate based mixes, regardless of the activator modulus. While in the case of olivine nano-silica based samples, there is an obvious increase of those sites when increasing the activator modulus.

3.4.3. ^{27}Al MAS NMR

Fig. 11(a) shows the ^{27}Al MAS NMR spectra of the unreacted slag and fly ash. Similar to other blast-furnace slags, the original slag presents a broad resonance between 0 and 80 ppm and centered at around 55 ppm. This broad peak region is assigned to a combination of Al(IV), Al(V) and Al(VI) sites [54,57], and cannot be identified as a single Al environment. This can be attributed to the distribution of Al environments within the glassy phase of slag, which shows a broad amorphous hump and almost undetectable crystalline phases (shown in XRD, Fig. 1). For the unreacted fly ash, a broad peak at around 46 ppm and a relatively narrow peak at around 2 ppm are identified, which are assigned to the tetrahedral and octahedral Al environment, respectively [58]. It has been reported that the resonance at around 2 ppm is assigned to the octahedral component in the mullite [54].

As shown in Fig. 11(b), after activation, all mixtures show a significant peak at around 64 ppm, and a narrow one with a relatively low intensity at about 10 ppm. The aluminate peak at 64 ppm is assigned to the tetrahedral Al(IV) that is incorporated in the Q2(1Al) and Q3(1Al) sites in C-A-S-H gels with bridging conditions [59,60], which is also proven by the ^{29}Si MAS NMR results in this study. It is also possible that a small amount of amorphous N-A-S-H type gels presents a contribution to this distorted Al(IV) region. The sharp peak centered at 10 ppm is commonly assigned to AFm and hydrotalcite type phases with octahedral coordination [53]. Besides, no other newly formed crystalline phases are observed in this binder system [32]. In this case, considering the identified crystalline phases (2 ppm with octa-Al) in the origin fly ash, and the relatively low content of fly ash in the total binder, the resonance centered at 10 ppm can be regarded as the hydrotalcite type phases resulting from the alkali activation of slag [61]. It should be noticed that these phases are usually poorly crystalized and formed in the interlayers of C-A-S-H gels, making it difficult to be detected by XRD [62], while the ^{27}Al MAS NMR verifies its presence. Besides, the unreacted slag and fly ash also contribute to the tetra-coordinated Al region (50 to 100 ppm), pentahedral region (30 to 40 ppm) and octahedral region (− 10 to 20 ppm). For a constant activator modulus, the difference in Al environments between olivine nano-silica based mixtures and commercial sodium silicate derived ones is rather small; with two obvious peaks that represent newly formed Al(IV) and Al(VI) sites, also their peak locations remain unchanged, indicating a very similar bonding environments surrounding the Al groups. Thus it is reasonable to conclude that the silica origin shows limited influence on the Al structures. When increasing the activator modulus, a slight decrease can be observed in the relative intensity of octahedral Al peak, compared to the tetrahedral one. It indicates that when the silicate content is increased in the system (from activator), more Al will participate into the C-A-S-H gels rather than form individual Al-rich phases.

3.5. Compressive strength

The 7 and 28 d compressive strengths of all mixtures are depicted in Table 7. It can be seen that for a fixed activator modulus, the olivine nano-silica based mixes exhibit comparable although very slightly lower compressive strengths as the commercial sodium silicate based ones. This phenomenon is in line with the isothermal calorimetry, thermogravimetry and ^{29}Si NMR results in this study, where the olivine

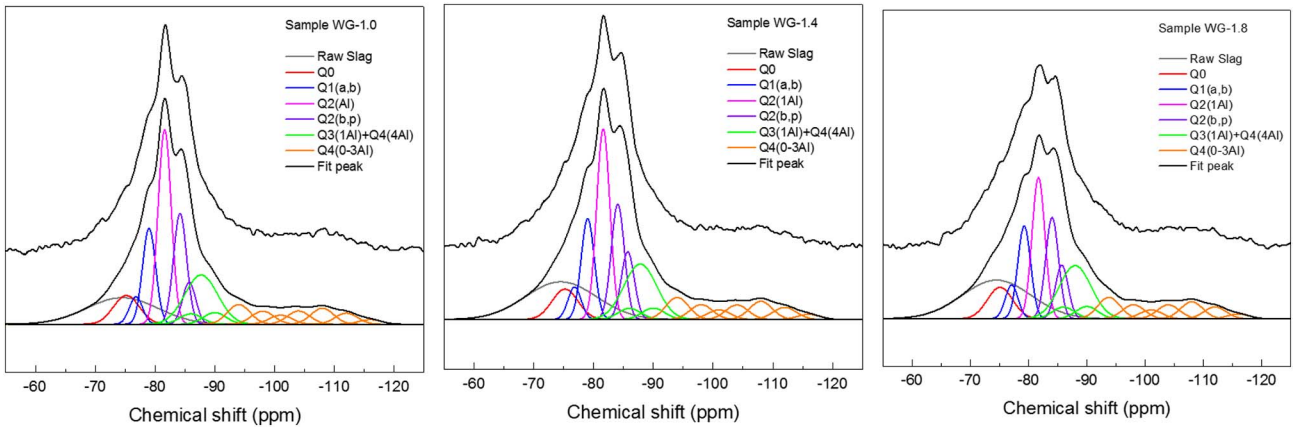

Fig. 10. ^{29}Si MAS NMR of mixes based on commercial waterglass.

Table 6
Summary of the deconvolution results fom ^{29}Si MAS NMR analysis. (%)

Chemical shift (ppm, ± 0.5)	Sample ID	NS-1.0	NS-1.4	NS-1.8	WG-1.0	WG-1.4	WG-1.8
− 55 to − 95	Unreacted slag	15.2	19.3	20.5	14.6	18.2	20.3
	Slag reactivity	71.5	62.1	58.0	72.5	64.2	58.5
− 75.2	Q0	6.3	5.3	4.3	5.8	5.4	6.1
− 76.8	Q1-a	3.6	3.8	2.9	2.8	2.9	3.3
− 79.0	Q1-b	9.6	9.1	8.0	9.6	9.0	9.0
− 81.6	Q2(1Al)	19.0	16.0	12.6	19.8	17.1	13.8
− 84.2	Q2-b	10.9	7.6	10.0	11.3	10.3	9.9
− 85.7	Q2-p	5.7	6.6	4.6	4.3	6.1	5.2
− 88	Q3(1Al) + Q4(4Al)	14.3	16.8	20.4	16.4	16.0	16.9
− 94 to − 116	Q4(0-3Al)	15.5	15.6	16.7	15.3	15.0	15.5

nano-silica based mixtures present a less intensive reaction process and lower reaction degree of the starting materials, therefore less formed gels result in a lower mechanical property. It should be noticed that although lower strengths are presented, the differences are in overall within 5% of the corresponding sodium silicate based ones. Their 7 d strengths range from 57.4 MPa to 68.2 MPa and the 28 d strengths are from 72.9 MPa to 82.1 MPa, which meet various construction application requirements [63]. For mixes based on olivine nano-silica, the 7 d strength is 61.9 MPa with an activator modulus of 1.0, and it increases to 68.2 MPa when increasing the activator modulus to 1.4, a further increase of the modulus to 1.8 leads to a reduction of strength to 57.4 MPa.

A similar tendency is also shown in the strength at 28 d. The presence of the optimal strength may imply an optimum activator modulus in terms of strength. However, it is difficult to quantify this relation since several factors show a synergetic effect on compressive strength, such as the mineral composition, amorphous phase content and fineness of the starting materials, reaction degree, alkali concentration and curing conditions, etc. The TG analysis in this study shows that the additional silicate actually leads to a slight reduction of the reaction degree, thus the increased mechanical property due to the additional silicate could be an indication of the physical modification on the hardened matrix. It is concluded that ideal compressive strengths can be achieved by using suitable content of additional silicate, and olivine nano-silica is capable of providing excellent mechanical properties.

3.6. CO_2 footprint

An important driving force and potential benefit of applying this alternative silicate source is the reduction of the carbon emission of

Table 7
7 and 28 d compressive strengths of alkali activated slag-fly ash blends with different activator conditions.

Sample	Compressive strength (MPa)	
	7 d	28 d
WG-1.0	67.5 ± 1.8	82.4 ± 2.1
WG-1.4	70.6 ± 2.1	87.8 ± 2.5
WG-1.8	61.6 ± 1.6	75.5 ± 1.4
NS-1.0	61.9 ± 2.2	78.3 ± 1.9
NS-1.4	68.2 ± 2.7	82.1 ± 2.5
NS-1.8	57.4 ± 2.1	72.9 ± 2.6

Table 8
Calculation of CO_2 emissions based on a sample concrete mix (kg/m^3).

Mix	Mix proportions						CO_2 emissions	
	Binder	NaOH	Na_2O-$nSiO_2$	Nano-silica	Fine aggr.	Coarse aggr.	From activator	In total
WG-1.0	315 Slag	20.52	28.49	0	800	1000	82.44	188.16
WG-1.4	+	17.1	39.74	0			92.93	198.65
WG-1.8	135	13.64	51.35	0			103.82	209.54
NS-1.0	Fly ash	29.03	0	21.87			65.66	171.38
NS-1.4		29.03	0	30.51			69.66	175.38
NS-1.8		29.03	0	39.42			73.76	179.48
Ref	450 OPC	0	0	0			0	426.02

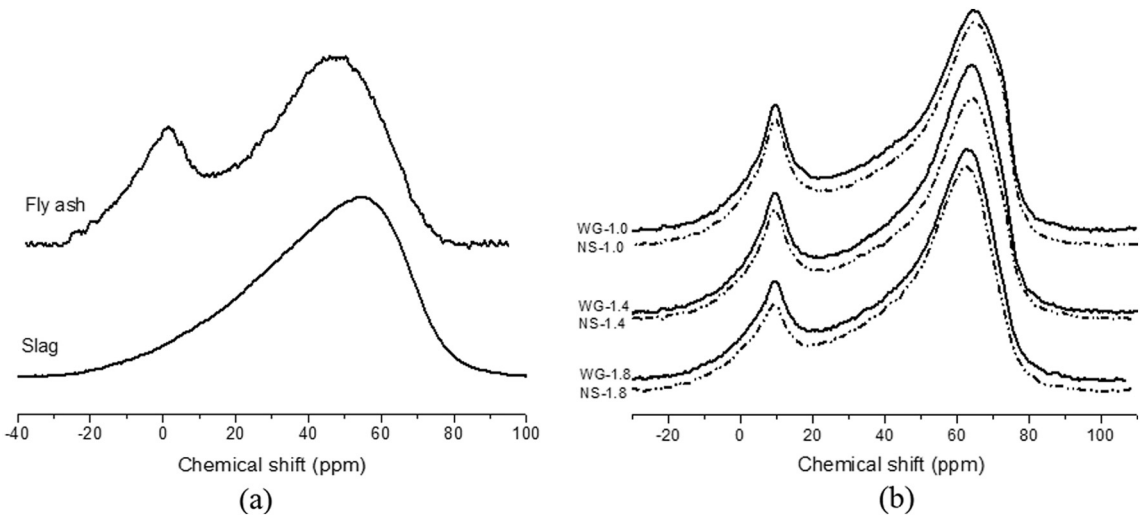

Fig. 11. ^{27}Al MAS NMR of starting materials and reaction products.

alkali activated binders. Therefore a calculation on the CO_2 footprint was carried out and the results are shown in Table 8. The carbon footprint is usually calculated as the sum of the CO_2 emissions of each component in unit volume of concrete. Considering that this value is highly related to the proportions of each particular component and the mix proportion of concrete can be largely varied; thus in this study, the evaluation is based on a given concrete recipe with a moderate binder content of 450 kg/m^3, and a Portland cement based sample is used as a reference. As listed in Table 8, the sodium silicate activator contains NaOH and commercial waterglass (Na_2O-nSiO_2-mH_2O), while the alternative activator consists of NaOH and olivine nano-silica (xSiO_2-yH_2O). Their corresponding contents are determined based on 450 kg/m^3 of binder, and those values are the effective solids contents excluding water. The carbon footprint used in this calculation: NaOH (1.915 tCO_2/t), commercial waterglass (1.514 tCO_2/t), OPC (0.82 tCO_2/t), slag (0.143 tCO_2/t), fly ash (0.027 tCO_2/t), fine aggregate (0.0139 tCO_2/t) and coarse aggregate (0.0459 tCO_2/t) are obtained from [64,65], while the CO_2 footprint of olivine nano-silica (0.461 tCO_2/t) was estimated from a life cycle analysis performed by VTT (EU F7th project, ProMine internal report) [66]. It is important to note that the carbon footprint for olivine nano-silica shown here is an average European industrial case scenario, without making use of the heat that is generated during the production of nano-silica, once this part of energy is reused, the carbon emission will be further reduced (see Eq. (1)). It should be mentioned that the nano-silica production data provided to the calculation is based mainly on laboratory and bench scale testing, and at this stage all amounts are based on reaction stoichiometric. The system boundary applied in the life cycle analysis (LCA) of the nano-silica production is shown in Fig. 12, and the supporting data sources for Fig. 12 are obtained from the listing institutes in Table 9.

The carbon footprint result used in this case (average European industrial scenario) is depicted in Fig. 13.

It can be seen from Table 8 that compared to the alkali activated material based concrete, the carbon emission of Portland cement concrete is more than doubled, indicating the clear benefit of using slag and fly ash as alternative binder in sustainable development. In terms of the alkali activated concrete, the carbon emission from the activator accounts for 43.8% to 49.5% of the total emission in commercial sodium silicate based mixes, and this value is about 38.3% to 41.1% in olivine nano-silica based ones, indicating a strong influence of activator in the total carbon emission. If concerning the activator alone, when olivine nano-silica is applied as the alternative silicate source, the carbon emission per 1 m^3 of concrete is reduced by 20.4%, 25.0% and 29.0% in mixes with an alkali activator modulus of 1.0, 1.4 and 1.8 respectively, compared to the commercial waterglass based ones. It is obvious that this reduction rate becomes higher when increasing the activator modulus. This is of great benefit since the alkali activated system usually requires additional silicate to improve its performance to a higher level, and when the olivine nano-silica is utilized to replace the commercial sodium silicate, a significantly reduced burden to the environment can be resulted. Moreover, the olivine nano-silica production could be still more sustainable if the heat produced during the reaction could be reused, the CO_2 footprint will be further reduced.

Table 9
Data source of the applied LCA analysis.

Process	Data source
Olivine production	Grecian magnesite
Nano-silica production	Selor
Chemicals: H_2SO_4 and MgO	VTT's KCL-EcoData
Electricity and heat	EcoInvent
Fuels	
Transportation	VTT's LIPASTO database

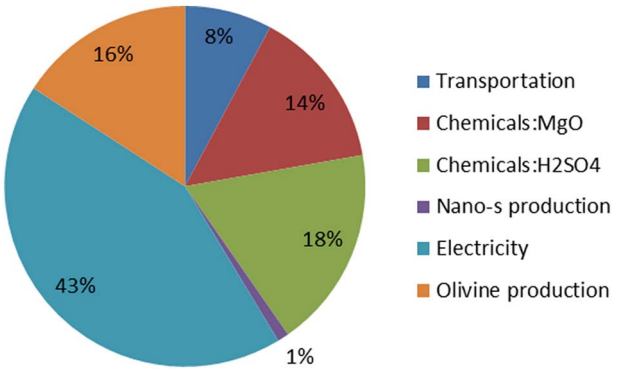

Fig. 13. Composition of the carbon footprint during nano silica preparation [66].

4. Conclusions

A green olivine nano-silica was synthesized and applied as an alternative alkali activator in alkali activated slag-fly ash blends; mixes with three different contents of additional silica were designed. Performance evaluations were carried out including activator characteristics, reaction kinetics, gel structure, compressive strength and CO_2 footprint. Comparisons were made with commercial sodium silicate based mixes. The following conclusions can be drawn based on the results:

- The olivine nano-silica is well dissolved in a NaOH solution to prepare activators with the same chemical composition as the

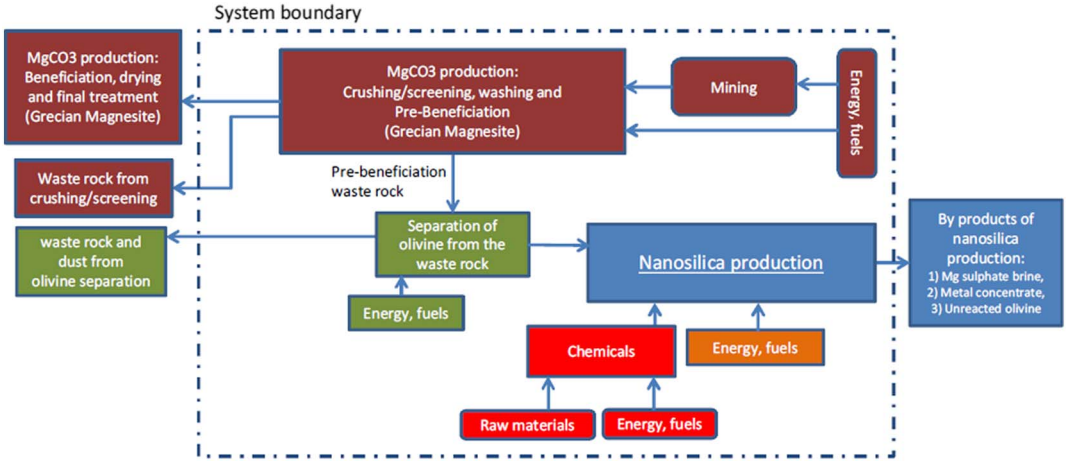

Fig. 12. System boundary of the applied LCA analysis [66].

sodium silicate based ones. The soluble silicate in the nano-silica based activators is above 99%; except the one with a modulus of 1.8, which nevertheless has a soluble silicate content of 98.1%. ^{29}Si NMR characterizations on the alkali solutions show that increasing the modulus results in an increased content of high cross-linking Q structures, and nano-silica based activators show a relatively high percentage of Q3 sites.

- For the same activator modulus, the olivine nano-silica based mixes present similar reaction process compared to the commercial waterglass based ones, with a slightly less intensity. Mixes with a higher activator modulus also exhibit a delayed early age reaction with reduced reaction intensity.
- Solid-state ^{29}Si and ^{27}Al MAS NMR together with TG verify that when increasing the activator modulus, the reactivity of slag is reduced, as well as the Al incorporation in C-A-S-H gels; nano-silica derived mixes show an increase of Q3(1Al) + Q4(4Al) sites, while those groups in commercial waterglass based ones remain stable. The nano-silica replacement results in a slightly reduced chemically bound water content and compressive strength, compared to the sodium silicate based mixes.
- The investigation on the effect of activator modulus reveals both physical and chemical modification of the additional silicates from the activator, and an optimum compressive strength is observed in mixes prepared with an activator modulus of 1.4.
- Alkali activated binders show greatly lower CO_2 compared to Portland cement. When olivine nano-silica is used as an alternative silicate source, the CO_2 emission from activator is reduced by 20.4% to 29.0% within the activator modulus range of 1.0 to 1.8; indicating a significant advantage towards carbon emission. In addition, the total CO_2 footprint can be further lower if the high amount of energy generated during the production of olivine nano-silica can be reused.

Acknowledgements

This research was supported by China Scholarship Council and the Department of the Built Environment at Eindhoven University of Technology (201306950046). The authors gratefully thank Prof. Dr. F.Z. Wang and Prof. Dr. W. Chen at Wuhan University of Technology (China) for supporting with the NMR experiments. The authors gratefully thank Mr. P. de Vries (ENCI B.V., the Netherlands) for the materials supply. Furthermore, the authors wish to express their gratitude to the following sponsors of the Building Materials research group at TU Eindhoven: Rijkswaterstaat Grote Projecten en Onderhoud; Graniet-Import Benelux; Kijlstra Betonmortel; Struyk Verwo; Attero; Enci; Rijkswaterstaat Zee en Delta-District Noord; Van Gansewinkel Minerals; BTE; V.d. Bosch Beton; Selor; GMB; Icopal; BN international; Eltomation, Knauf Gips; Hess AAC Systems; Kronos; Joma; CRH Europe Sustainable Concrete Centre; Cement & Beton Centrum; Heros; Inashco; Keim; Sirius International and Boskalis (in chronological order of joining).

References

[1] C.J. Shi, A. Fernández Jiménez, A. Palomo, New cements for the 21st century: the pursuit of an alternative to Portland cement, Cem. Concr. Res. 41 (2011) 750–763.
[2] A.M. Rashad, A comprehensive overview about the influence of different additives on the properties of alkali-activated slag - a guide for civil engineer, Constr. Build. Mater. 47 (2013) 29–55.
[3] S.D. Wang, K.L. Scrivener, P.L. Pratt, Factors affecting the strength of alkali-activated slag, Cem. Concr. Res. 24 (6) (1994) 1033–1043.
[4] A. Fernández-Jiménez, I. García-Lodeiro, A. Palomo, Durable characteristics of alkali activated fly ashes, J. Mater. Sci. 42 (2007) 3055–3065.
[5] D.M.A. Huiskes, A. Keulen, Q.L. Yu, H.J.H. Brouwers, Design and performance evaluation of ultra-lightweight geopolymer concrete, Mater. Des. 89 (2016) 516–526.
[6] B. Yuan, Q.L. Yu, H.J.H. Brouwers, Reaction kinetics, reaction products and compressive strength of ternary activators activated slag designed by Taguchi method, Mater. Des. 86 (2015) 878–886.
[7] A.R. Brough, A. Atkinson, Sodium silicate-based alkali-activated slag mortars: part I. Strength, hydration and microstructure, Cem. Concr. Res. 32 (2002) 865–879.
[8] Li Chao, Sun Henghu, Li Longtu, A review: the comparison between alkali-activated slag (Si + Ca) and metakaolin (Si + Al) cements, Cem. Concr. Res. 40 (2010) 1341–1349.
[9] N.K. Lee, H.K. Lee, Setting and mechanical properties of alkali-activated fly ash/slag concrete manufactured at room temperature, Constr. Build. Mater. 47 (2013) 1201–1209.
[10] Alaa M. Rashad, Properties of alkali-activated fly ash concrete blended with slag, Iran. J. Mater. Sci. Eng. 10 (1) (2013) 57–64.
[11] S. Aydin, A ternary optimization of mineral additives of alkali activated cement mortars, Constr. Build. Mater. 43 (2013) 131–138.
[12] T. Sugama, L.E. Brothers, T.R. Van de Putte, Acid-resistant cements for geothermal wells: sodium silicate activated slag/fly ash blends, Adv. Cem. Res. 17 (2) (2005) 65–75.
[13] C.K. Yip, G.C. Lukey, J.S.J. van Deventer, The coexistence of geopolymeric gel and calcium silicate hydrate at the early stage of alkaline activation, Cem. Concr. Res. 35 (2005) 1688–1697.
[14] I. García-Lodeiro, D.E. Macphee, A. Palomo, A. Fernández-Jiménez, Effect on fresh C-S-H gels the simultaneous addition of alkali and aluminium, Cem. Concr. Res. 40 (2010) 27–32.
[15] I. Ismail, S.A. Bernal, J.L. Provis, R.S. Nicolas, S. Hamdan, J.S.J. Deventer, Modification of phase evolution in alkali-activated blast furnace slag by the incorporation of fly ash, Cem. Concr. Compos. 45 (2014) 125–135.
[16] X. Gao, Q.L. Yu, H.J.H. Brouwers, Characterization of alkali activated slag-fly ash blends containing nano-silica, Constr. Build. Mater. 98 (2015) 397–406.
[17] M. Chi, R. Huang, Binding mechanism and properties of alkali-activated fly ash/slag mortars, Constr. Build. Mater. 40 (2013) 291–298.
[18] F. Puertas, S. Martínez-Ramírez, S. Alonso, E. Vázquez, Alkali-activated fly ash/slag cement. Strength behaviour and hydration products, Cem. Concr. Res. 30 (2000) 1625–1632.
[19] S.A. Bernal, J.L. Provis, V. Rose, A. Mejía de Gutierrez, Evolution of binder structure in sodium silicate-activated slag-metakaolin blends, Cem. Concr. Compos. 33 (2011) 46–54.
[20] X. Gao, Q.L. Yu, H.J.H. Brouwers, Assessing the porosity and shrinkage of alkali activated slag-fly ash composites designed applying a packing model, Constr. Build. Mater. 119 (2016) 175–184.
[21] F. Puertas, M. Torres-Carrasco, Use of glass waste as an activator in the preparation of alkali-activated slag. Mechanical strength and paste characterization, Cem. Concr. Res. 57 (2014) 95–104.
[22] P. Duxson, J.L. Provis, G.C. Lukey, S.W. Mallicoat, W.M. Kriven, J.S.J. Deventer, Understanding the relationship between geopolymer composition, microstructure and mechanical properties, Colloids Surf. A Physicochem. Eng. Asp. 269 (2005) 47–58.
[23] B.C. McLellan, R.P. Williams, J. Lay, A. van Riessen, G.D. Corder, Costs and carbon emissions for geopolymer pastes in comparison to ordinary portland cement, J. Clean. Prod. 19 (2011) 1080–1090.
[24] European Commission, Reference Document on Best Available Techniques for the Manufacture of Large Volume Inorganic Chemicals – Solids and Others Industry, (2007).
[25] A. Lazaro, Nano-silica Production at Low Temperatures From the Dissolution of Olivine (Ph.D. Thesis), Eindhoven University of Technology, The Netherlands, 2014, pp. 1–225.
[26] E.D. Rodríguez, S.A. Bernal, J.L. Provis, J. Paya, J.M. Monzo, M.V. Borrachero, Effect of nanosilica-based activators on the performance of an alkali-activated fly ash binder, Cem. Concr. Compos. 35 (2013) 1–11.
[27] V. Zivica, Effectiveness of new silica fume alkali activator, Cem. Concr. Compos. 28 (2006) 21–25.
[28] S.A. Bernal, E.D. Rodriguez, R.M. Gutierrez, J.L. Provis, S. Delvasto, Activation of metakaolin/slag blends using alkaline solutions based on chemically modified silica fume and rice husk ash, Waste Biomass Valoriz. 3 (2012) 99–108.
[29] A. Lazaro, H.J.H. Brouwers, G. Quercia, J.W. Geus, The properties of amorphous nano-silica synthesized by the dissolution of olivine, Chem. Eng. J. 211 (2012) 112–121.
[30] A. Lazaro, M.C. van de Griend, H.J.H. Brouwers, J.W. Geus, The influence of process conditions and Ostwald ripening on the specific surface area of olivine nano-silica, Microporous Mesoporous Mater. 181 (2013) 254–261.
[31] X. Gao, Q.L. Yu, H.J.H. Brouwers, Reaction kinetics, gel character and strength of ambient temperature cured alkali activated slag-fly ash blends, Constr. Build. Mater. 80 (2015) 105–115.
[32] X. Gao, Q.L. Yu, H.J.H. Brouwers, Properties of alkali activated slag-fly ash blends with limestone addition, Cem. Concr. Compos. 59 (2015) 119–128.
[33] British standard EN 196-1:2005. Methods of testing cement part 1: determination of strength.
[34] A. Lazaro, G. Quercia, H.J.H. Brouwers, J.W. Geus, Synthesis of a green nano-silica material using beneficiated waste dunites and its application in concrete, World J. Nano Sci. Eng. 3 (2013) 41–51.
[35] R.A. Robie, B.S. Hemingway, H. Takei, Heat capacities and entropies of Mg_2SiO_4, Mn_2SiO_4, and Co_2SiO_4 between 5 and 380 K, Am. Mineral. 67 (1982) 470–482.
[36] R.K. Iler, The Chemistry of Silica: Solubility, Polymerization, Colloid and Surface Properties, and Biochemis- try, John Wiley and Sons, New York, 1979.
[37] J.L. Provis, J.S.J. van Deventer, Geopolymers: Structure, Processing, Properties and Industrial Applications, Woodhead Publishing Limited, 2009, p. 59.
[38] H. Jansson, D. Bernin, K. Ramser, Silicate species of water glass and insights for alkali-activated green cement, AIP Adv. 5 (2015) 067167.
[39] S.A. Bernal, J.L. Provis, B. Walkerly, et al., Gel nanostructure in alkali-activated

binders based on slag and fly ash, and effects of accelerated carbonation, Cem. Concr. Res. 53 (2013) 127–144.
[40] S.A. Bernal, et al., MgO content of slag controls phase evolution and structural changes induced by accelerated carbonation in alkali-activated binders, Cem. Concr. Res. 57 (2014) 33–43.
[41] X.L. Pardal, F. Brunet, T. Charpentier, I. Pochard, A. Nonat, ^{27}Al and ^{29}Si solid-state NMR characterization of calcium-aluminosilicate-hydrate, Inorg. Chem. 51 (2012) 1827–1836.
[42] E. Lhopital, B. Lothenbach, G. Saout, D. Kulik, K.L. Scrivener, Incorporation of aluminium in calcium-silicate-hydrates, Cem. Concr. Res. 75 (2015) 91–103.
[43] E. Deira, B.S. Gebregziabiher, S. Peethamparan, Influence of starting material on the early age hydration kinetics, microstructure and composition of binding gel in alkali activated binder systems, Cem. Concr. Compos. 48 (2014) 108–117.
[44] S. Chithiraputhiran, N. Neithalath, Isothermal reaction kinetics and temperature dependence of alkali activation of slag, fly ash and their blends, Constr. Build. Mater. 45 (2013) 233–242.
[45] A.R. Brough, M. Holloway, J. Sykes, A. Atkinson, Sodium silicate-based alkali-activated slag mortars part II. The retarding effect of additions of sodium chloride or malic acid, Cem. Concr. Res. 30 (2000) 1375–1379.
[46] D. Ravikumar, N. Neithalath, Reaction kinetics in sodium silicate powder and liquid activated slag binders evaluated using isothermal calorimetry, Thermochim. Acta 546 (2012) 32–43.
[47] C. Shi, R.L. Day, A calorimetric study of early hydration of alkali-slag cements, Cem. Concr. Res. 25 (1995) 1333–1346.
[48] T. Bakharev, J.G. Sanjayan, Y.B. Cheng, Alkali activation of Australian slag cements, Cem. Concr. Res. 29 (1) (1999) 113–120.
[49] D. Krizana, B. Zivanovic, Effects of dosage and modulus of water glass on early hydration of alkali–slag cements, Cem. Concr. Res. 32 (2002) 1181–1188.
[50] M. Criado, A. Fernandez-Jimenez, A. Palomo, I. Sobrados, J. Sanz, Effect of the SiO^2/Na^2O ratio on the alkali activation of fly ash. Part II: ^{29}Si MAS-NMR survey, Microporous Mesoporous Mater. 109 (2008) 525–534.
[51] L. Alarcon-Ruiz, G. Platret, E. Massieu, A. Ehrlacher, The use of thermal analysis in assessing the effect of temperature on a cement paste, Cem. Concr. Res. 35 (2005) 609–613.
[52] P. Rovnaník, P. Bayer, P. Rovnaníková, Characterization of alkali activated slag paste after exposure to high temperatures, Constr. Build. Mater. 47 (2013) 1479–1487.
[53] S.D. Wang, K.L. Scrivener, ^{29}Si and ^{27}Al NMR study of alkali-activated slag, Cem. Concr. Res. 33 (5) (2003) 769–774.
[54] A. Palomo, S. Alonso, A. Fernandez, A. Sobrados, J. Sanz, Alkaline activation of fly ashes: NMR study of the reaction products, J. Am. Ceram. Soc. 87 (6) (2004) 1141–1145.
[55] R.J. Myers, S.A. Bernal, R.S. Nicolas, J.L. Provis, Generalized structural description of calcium-sodium aluminosilicate hydrate gels: the cross-linked substituted tobermorite model, Langmuir 29 (2013) 5294–5306.
[56] I.G. Richardson, The calcium silicate hydrates, Cem. Concr. Res. 38 (2008) 137–158.
[57] L.H. Merwin, A. Sebald, H. Rager, H. Schneider, ^{29}Si and ^{27}Al MAS NMR spectroscopy of mullite, Phys. Chem. Miner. 18 (1991) 47–52.
[58] G.K. Sun, J.F. Young, R.J. Kirkpatrick, The role of Al in C-S-H: NMR, XRD, and compositional results for precipitated samples, Cem. Concr. Res. 36 (1) (2006) 18–29.
[59] P. Faucon, A. Delagrave, J.C. Petit, C. Richet, J.M. Marchand, H. Zanni, Aluminum incorporation in calcium silicate hydrates (C-S-H) depending on their Ca/Si ratio, J. Phys. Chem. B 103 (37) (1999) 7796–7802.
[60] G.L. Saout, M.B. Haha, F. Winnefeld, B. Lothenbach, Hydration degree of alkali-activated slags: a ^{29}Si NMR study, J. Am. Ceram. Soc. 94 (2011) 4541–4547.
[61] K.J.D. MacKenzie, R.H. Meinhold, B.L. Sherriff, Z. Xu, ^{27}Al and ^{25}Mg solid-state magic-angle spinning nuclear magnetic resonance study of hydrotalcite and its thermal decomposition sequence, J. Mater. Chem. 3 (12) (1993) 1263–1269.
[62] P.J. Schilling, L.G. Butler, A. Roy, A.H. Eaton, ^{29}Si and ^{27}Al MAS-NMR of NaOH activated blast-furnace slag, J. Am. Ceram. Soc. 77 (9) (1994) 2363–2368.
[63] S. Minderss, J.F. Young, D. Darwin, Concrete, second edition, Prentice Hall, Pearson Education, Inc, 2003.
[64] F. Collins, Inclusion of carbonation during the life cycle of built and recycled concrete: influence on their carbon footprint, Int. J. Life Cycle Assess. 15 (2010) 549–556.
[65] L.K. Turner, F.G. Collins, Carbon dioxide equivalent (CO_2-e) emissions: a comparison between geopolymer and OPC cement concrete, Constr. Build. Mater. 43 (2013) 125–130.
[66] EU FP7 project ProMine: Nanoparticle products from new mineral resources in Europe (Grant agreement No. 228559).
[67] R.H. Perry, Green DW, McGraw-Hill, Perry's chemical engineers' handbook, 2008.